Decreasing Collectivity in Smoothly Terminating Bands in the $A \sim 110$ Region

R. Wadsworth,[1] R. M. Clark,[2] J. A. Cameron,[3] D. B. Fossan,[4] I. M. Hibbert,[1] V. P. Janzen,[5] R. Krücken,[2] G. J. Lane,[4] I. Y. Lee,[2] A. O. Macchiavelli,[2] C. M. Parry,[1] J. M. Sears,[4] J. F. Smith,[4] A. V. Afanasjev,[6,*] and I. Ragnarsson[6]

[1]*Department of Physics, University of York, Heslington, York, YO1 5DD, United Kingdom*
[2]*Nuclear Science Division, Lawrence Berkeley National Laboratory, Berkeley, California 94720*
[3]*Department of Physics and Astronomy, McMaster University, Hamilton, Ontario, Canada L8S 4M1*
[4]*Department of Physics and Astronomy, SUNY at Stony Brook, Stony Brook, New York 11794-3800*
[5]*Chalk River Laboratories, Atomic Energy of Canada Ltd., Chalk River, Ontario, Canada K0J 1J0*
[6]*Department of Mathematical Physics, Lund Institute of Technology, P.O. Box 118, S-22100 Lund, Sweden*

(Received 15 September 1997)

Lifetimes of states in two rotational bands in ^{108}Sn and one in ^{109}Sb have been determined using the Doppler shift attenuation method. The deduced quadrupole moments for the states are in excellent agreement with cranked Nilsson model predictions, which imply a gradual change in the nuclear shape from collective near-prolate at medium spin to noncollective oblate at high spin. This change results from the gradual alignment of the spin vectors of the valence particles and holes in a specific configuration. These data provide crucial evidence in support of the phenomenon of smooth band termination. [S0031-9007(97)05258-7]

PACS numbers: 21.10.Tg, 21.10.Ky, 21.10.Re, 27.60.+j

The nuclei in the $A \sim 110$ mass region have revealed some surprising nuclear structure features in recent years. In the tin isotopes, rotational bands arising from proton two-particle–two hole (2p-2h) excitations across the $Z = 50$ shell gap [1,2] coexist with single-particle states at moderate spin. These 2p-2h structures have a quadrupole deformation of $\varepsilon_2 = 0.20 - 0.25$ induced through the promotion of protons from the up-sloping (with increasing ε_2) $\pi g_{9/2}$ orbital into the down-sloping $\pi(g_{7/2}, d_{5/2})$ or $\pi h_{11/2}$ orbitals. In the Sb isotopes ($Z = 51$), the corresponding bands are based on a 3p-2h proton structure [3–5]. At higher frequencies, as the valence nucleons align their spin vectors with the axis of rotation, the structures in nuclei around $A \sim 110$ display a unique feature, whereby the dynamic moments of inertia, $\mathcal{J}^{(2)}$, gradually decrease with increasing spin to unusually low values, typically about one-third of the rigid body value. Moreover, the energy of the last few states in the bands is observed to increase rather than decrease when a rotating liquid drop reference energy is subtracted ($E - E_{\mathrm{RLD}}$). In addition, several of these bands have been observed to have a sharp falloff in intensity for the last transition.

These intriguing features have been interpreted using configuration-dependent cranked Nilsson calculations [6,7], which indicate that, as the spin vectors of the available valence nucleons outside the $Z = N = 50$ double-shell closure align, the nuclear shape gradually traces a path through the triaxial plane from a collective near-prolate shape ($\gamma \sim 0°$, Lund convention [8]) to a noncollective oblate shape ($\gamma = +60°$) over many transitions (see Fig. 1). The band-termination spin for a specific configuration is equal to the sum of the aligned spins of the valence particles and holes. This feature has been called *smooth band termination* in order to contrast it with the shorter and more irregular terminating bands seen in nuclei such as ^{158}Er [9,10]. The reason why the bands in the $A \sim 110$ region can be followed to, or close to, termination is because they are yrast or near yrast over a large spin range.

The high-spin experimental properties of these terminating band structures are in remarkable agreement

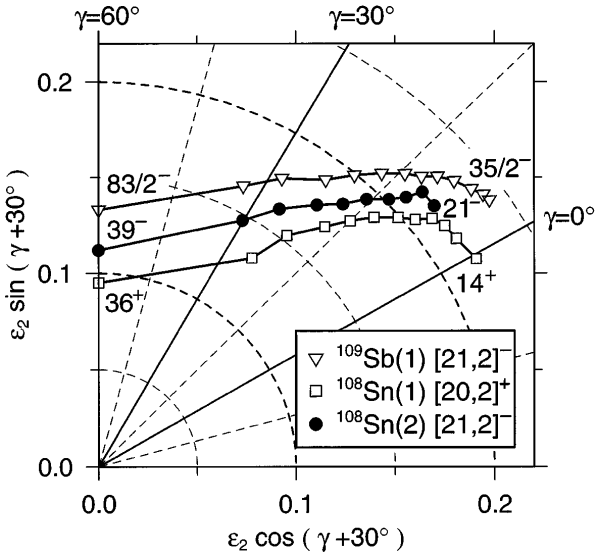

FIG. 1. Calculated deformations (ε_2 and γ) for the $[20, 2]^+$ (band 1) and $[21, 2]^-$ (band 2) configurations in ^{108}Sn and the $[21, 2]^-$ (band 1) configuration in ^{109}Sb as a function of spin in steps of $2\hbar$. {The notation used is $[p_1 p_2, n]^{\alpha_{\mathrm{tot}}}$, where p_1 and p_2 are the number of holes and particles in the proton $g_{9/2}$ and $h_{11/2}$ orbitals, respectively, n is the number of neutrons in the $h_{11/2}$ orbital, and α_{tot} is the total signature: the remaining orbitals outside ^{100}Sn being $(g_{7/2}, d_{5/2})$.} Note the gradual transition from a collective near-prolate ($\gamma \sim 0°$) shape to a noncollective oblate ($\gamma = +60°$) shape as the spin increases.

 0031-9007/98/80(6)/1174(4)$15.00

with the cranked Nilsson model calculations. A crucially important prediction, however, remains to be experimentally validated: The collectivity of these bands is expected to decrease as the band spin increases towards termination [6,7]. In order to test the predicted decreasing collective quadrupole moments and $B(E2)$ transition probabilities with increasing spin, an experiment has been performed to obtain, for the first time, the individual state lifetimes and quadrupole moments for two terminating bands in ^{108}Sn (bands 1 and 2 [1]) and one band in ^{109}Sb (band 1 [3,4]) (see Fig. 1).

High spin states in ^{109}Sb and ^{108}Sn were populated using the ^{54}Fe(^{58}Ni, xp) reactions ($x = 3, 4$) at a beam energy of 243 MeV. The beam, which was provided by the 88-inch cyclotron at the Lawrence Berkeley National Laboratory, was incident on a 600 μg/cm^2 thick, enriched, ^{54}Fe target foil on a 15.2 mg/cm^2 gold backing. Lifetimes of states in the 2p-2h bands were obtained using the Doppler shift attenuation method [11], which relies on a knowledge of the initial velocity distribution of the recoiling nuclei and the time scale of the nuclei slowing down and stopping in the target and backing material. A smaller data set was also collected using a self-supporting 500 μg/cm^2 ^{54}Fe target. These latter data were used to extract the intensities of the transitions within the bands. Gamma rays were detected using the Gammasphere array [12] which consisted of 95 hyperpure large volume germanium detectors. A total of 2.5×10^9 quadruple and higherfold gamma coincidence events were collected in the backed target experiment. The data were decomposed into $E_\gamma - E_\gamma - E_\gamma$ events and sorted into gated $E_\gamma - E_\gamma$ correlation matrices. This was achieved by gating on several transitions located below, and in coincidence with, the bands and, if possible, γ rays at the bottom of the bands. Only transitions with no Doppler shifted component were used as gates. One axis of the matrices contained all detectors while the other axis contained detectors at specific angles. In order to produce matrices with sufficient statistics, it was necessary to add together detectors located in certain adjacent angles to produce composite angles. The combinations (number of detectors) used were 79.2°(5) and 80.7°(4) giving 79.9°, 99.3°(5)/100.8°(3) → 99.9°, 121.7°(5)/129.9°(10) → 127.2°, 50.7°(8)/58.3°(4) → 53.2°, 32.7°(5)/37.4°(5) → 35.1°, and 142.6°(5)/148.3°(5) → 145.5°. Additional detectors were located at 17.3°(5), 69.8°(6), 90°(8), 110.2°(7), and 162.7°(5).

Spectra were projected onto the composite angle axis using the cleanest gates. The resulting spectra yielded Doppler broadened line shapes in the region 750–1150 keV and Doppler shifted transitions at higher energies. Lifetimes of states within the bands were extracted from these Doppler shifts using the analysis package of Wells and Johnson [13], and the energy loss was modeled using the prescription of Gascon *et al.* [14]. Shell corrections were applied to the electronic stopping powers of Northcliffe and Schilling [15] following the prescription of Ward [16]. The detailed slowing down history of the recoils in the target and backing material was simulated using a Monte Carlo technique, which involved 10 000 histories with a time step of 0.002 ps, and the results sorted according to detector geometry. The calculated average time taken to stop the recoils was approximately 1.3 ps. Calculated line shapes were produced assuming both feeding into the top of the band, which was simulated through a rotational cascade of five transitions with a similar moment of inertia to that of the band itself, and sidefeeding into each state. The sidefeeding intensity was constrained to be the same as that deduced experimentally from the thin target data. Fits were made to spectra from three different angles simultaneously. These included various combinations of forward and backward detectors and detectors situated at 90°, the latter of which were particularly useful for locating contaminants. The effective lifetime of the highest transition observed in each band was determined and used as an input parameter to obtain the lifetimes of states lower in the bands. Final results were obtained by fitting up to six members of a band simultaneously with independent variable lifetimes for each state. The lifetime of the associated sidefeeding was also varied and simulated using a rotational cascade of five transitions for most of the states in the bands. Furthermore, the dynamic moment of inertia, $\mathcal{J}^{(2)}$, of the sidefeeding cascade was varied to check that this did not significantly affect the results. In this case, the in-band levels were observed to have similar lifetimes to those quoted in Table I. For the lowest two or three levels in each band, both independent multiple single-step feeding and rotational cascade feeding were tried. The former method yielded slightly better fits to the data. In this case, five independent levels were used whose lifetimes were all variable. In general, the sidefeeding lifetimes were found to be 1–3 times faster than the in-band lifetimes. Figure 2 shows the experimental data, together with the best calculated fits, for four transitions from band 1 in ^{109}Sb.

Band 1 in ^{108}Sn is crossed at high spin by another structure which has the same parity and signature [see inset to Fig. 3(b)]. The 1895 keV linking transition was strong enough to extract an effective lifetime. This yielded a value which was the same, within errors, as the sidefeeding time deduced for the 1704 keV transition in band 1. Since the 1895 keV γ ray accounts for more than 50% of the sidefeeding into this state this is a good cross check that the sidefeeding lifetimes obtained are reasonable.

The lifetimes of the states in the $[20, 2]^+$ band 1 and $[21, 2]^-$ band 2 of ^{108}Sn and the $[21, 2]^-$ band 1 of ^{109}Sb are summarized in Table I (for notation, see the caption of Fig. 1). The errors are determined primarily from the spread in the results from fitting the lifetimes to different angle data. They also reflect the behavior of the χ^2 in the neighborhood of the best fit for each angle combination used; however, they do not include systematic errors which are inherent in the stopping powers used, and

TABLE I. Gamma ray energies, spins of initial states from which the γ rays depopulate, sidefeeding intensities, lifetimes, and reduced transition strengths for states in the three bands. All γ-branching ratios were 1.0 unless explicitly stated.

	E_γ (keV)	J_i^π	I_{SF} (%)	τ (ps)	$B(E2)$ $(e^2\,b^2)$
^{109}Sb(1)	791	$\frac{39}{2}^-$	0	$0.648^{+0.088}_{-0.071}$	$0.365^{+0.042}_{-0.051}$ [a]
	861	$\frac{43}{2}^-$	12(3)	$0.409^{+0.046}_{-0.033}$	$0.421^{+0.034}_{-0.047}$
	977	$\frac{47}{2}^-$	14(3)	$0.253^{+0.032}_{-0.027}$	$0.362^{+0.039}_{-0.046}$
	1093	$\frac{51}{2}^-$	15(3)	$0.149^{+0.015}_{-0.014}$	$0.351^{+0.033}_{-0.035}$
	1203	$\frac{55}{2}^-$	13(4)	$0.107^{+0.012}_{-0.014}$	$0.302^{+0.040}_{-0.034}$
	1326	$\frac{59}{2}^-$	8(5)	$0.062^{+0.006}_{-0.008}$	$0.321^{+0.041}_{-0.032}$
	1476	$\frac{63}{2}^-$	19(5)	$0.051^{+0.009}_{-0.008}$	$0.228^{+0.036}_{-0.040}$
	1648	$\frac{67}{2}^-$	42(8)	$0.031^{+0.007}_{-0.007}$	$0.216^{+0.049}_{-0.049}$
	1849	$\frac{71}{2}^-$	60(10)	$0.029^{+0.007}_{-0.007}$	$0.130^{+0.031}_{-0.031}$
	2097	$\frac{75}{2}^-$	60(10)	$0.019^{+0.006}_{-0.005}$	$0.106^{+0.033}_{-0.028}$
^{108}Sn(1)	791	16^+	10(3)	$0.947^{+0.148}_{-0.151}$	$0.278^{+0.044}_{-0.043}$
	901	18^+	10(3)	$0.540^{+0.084}_{-0.090}$	$0.254^{+0.042}_{-0.040}$
	1014	20^+	15(4)	$0.310^{+0.041}_{-0.042}$	$0.245^{+0.032}_{-0.032}$
	1119	22^+	15(4)	$0.202^{+0.038}_{-0.034}$	$0.230^{+0.039}_{-0.043}$
	1225	24^+	15(5)	$0.137^{+0.031}_{-0.018}$	$0.216^{+0.029}_{-0.049}$
	1356	26^+	22(5)	$0.077^{+0.013}_{-0.009}$	$0.231^{+0.027}_{-0.039}$
	1514	28^+	30(6)	$0.056^{+0.011}_{-0.011}$	$0.183^{+0.036}_{-0.036}$
	1704	30^+	65(10)	$0.047^{+0.016}_{-0.012}$	$0.121^{+0.031}_{-0.041}$
^{108}Sn(2)	948	23^-	0	$0.440^{+0.064}_{-0.060}$	$0.218^{+0.030}_{-0.032}$ [a]
	1042	25^-	0	$0.270^{+0.036}_{-0.036}$	$0.246^{+0.033}_{-0.033}$
	1180	27^-	20(4)	$0.159^{+0.023}_{-0.021}$	$0.224^{+0.030}_{-0.032}$
	1356	29^-	15(5)	$0.082^{+0.014}_{-0.010}$	$0.217^{+0.026}_{-0.037}$
	1542	31^-	40(8)	$0.051^{+0.008}_{-0.007}$	$0.183^{+0.025}_{-0.029}$
	1741	33^-	50(12)	$0.030^{+0.006}_{-0.006}$	$0.170^{+0.034}_{-0.034}$
	1982	35^-	66(15)	$0.023^{+0.007}_{-0.007}$	$0.116^{+0.035}_{-0.035}$

[a]Experimental γ-branching ratios of 0.9 were used in each case.

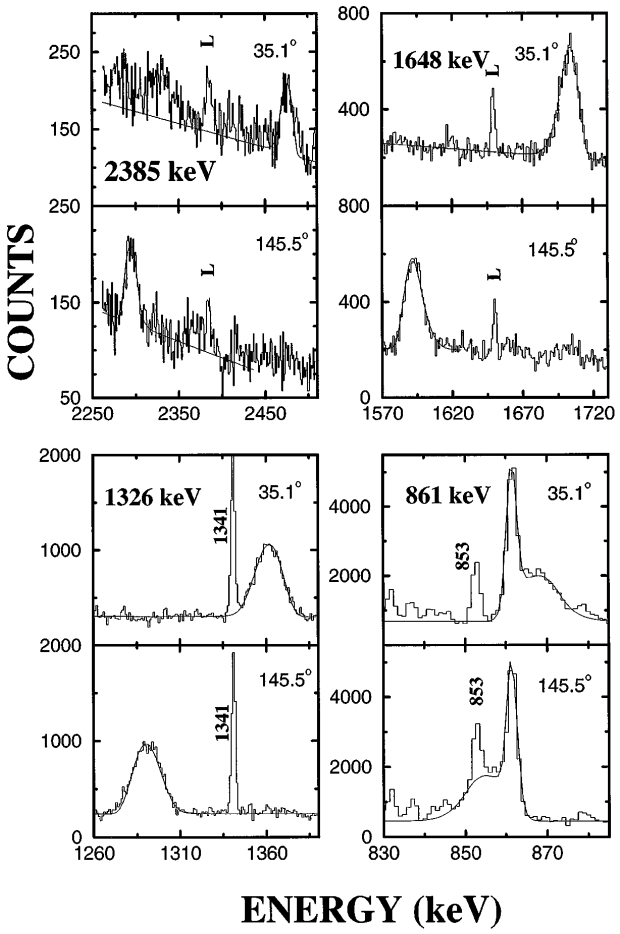

FIG. 2. Experimental data and associated line-shape fits for the 2385, 1648, 1326, and 861 keV transitions in band 1 of ^{109}Sb. The spectra result from summing together projections obtained by gating on the 806 and 593 keV fully stopped feed-out transitions below the band. These projections were taken from matrices which had been created using gates on several transitions which are below, and in coincidence with, band 1 (Fig. 3 of Ref. [4]). Composite angles for the detectors used to create the spectra are shown in the top right-hand corner of each box. Stopped transitions marked with an L are linking transitions from the bottom of the band to the spherical states. The 853 and 1341 keV γ-rays are low-lying transitions from spherical states at the bottom of the ^{109}Sb decay scheme.

which could be as large as $\pm 15\%$. Table I also contains the experimental side feeding intensities and the deduced $B(E2)$ values.

Figure 3 shows the experimentally deduced transition quadrupole moments Q_t for each state, and compares them with the values calculated from the equilibrium deformations of corresponding states for the suggested configurations. The calculations were performed using the configuration-dependent shell correction approach plus the cranked Nilsson potential [17], with the generalization [6,7] which allows the identification of high-j orbitals in each N shell after diagonalization. This is done by locating the orbitals with the largest expectation value of j^2 at a low frequency and then following these diabatic orbitals for all frequencies. This technique distinguishes between the particles of approximate $g_{9/2}$ character and those belonging to other low-j subshells of the $N = 4$ oscillator shell. The calculations are carried out in a mesh in the deformation space $(\varepsilon_2, \varepsilon_4, \gamma)$. Then, for each fixed configuration and each spin separately, the total energy of the nucleus is determined by a minimization with respect to the shape degrees of freedom. Pairing correlations are neglected in the calculations, a feature motivated by the lack of expected quasiparticle alignments at $\hbar\omega \geq 0.6-0.7$ MeV in the observed bands [7]. The transition quadrupole moment Q_t is calculated from the equilibrium deformations $(\varepsilon_2, \varepsilon_4, \gamma)$ using Eq. 3–5 of Ref. [18].

The overall agreement between theory and experiment is remarkably good (see Fig. 3) and documents the

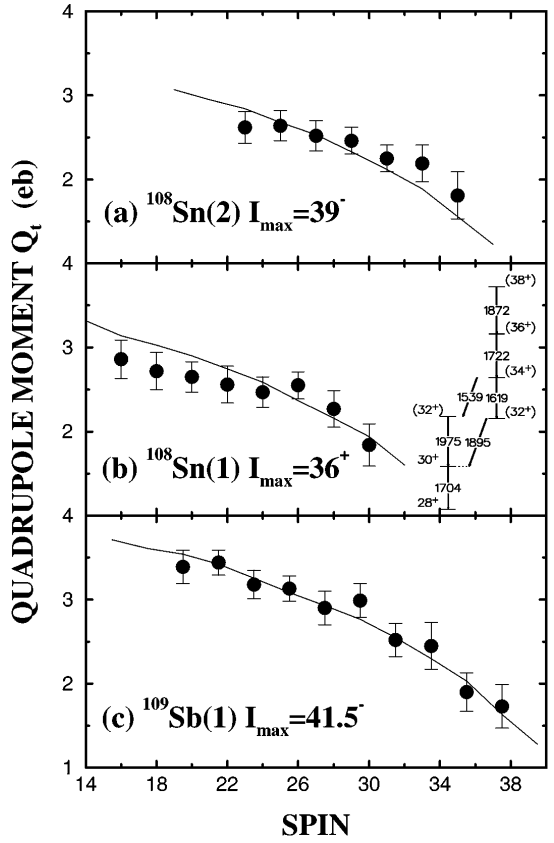

FIG. 3. Experimentally deduced transition quadrupole moments for (a) band 2 ($[21, 2]^-$), (b) band 1 ($[20, 2]^+$) in ^{108}Sn, (c) band 1 ($[21, 2]^-$) in ^{109}Sb (see Fig. 1 for notation). Solid lines represent the calculated values for these configurations and were obtained from the cranked Nilsson model. The inset in (b) shows the top of band 1 in ^{108}Sn and how it is crossed by what is thought to be the $[21, 3]^+$ terminating configuration (see Ref. [1] for further details).

decreasing collectivity of these bands as they gradually approach termination. This agreement is obtained without any "*a posteri*" adjustment of parameters. Indeed, the deformations were calculated previously (see Fig. 10, Ref. [4] and Fig. 5, Ref. [1]) and since the Q_t values depend on these, following the earlier theory techniques of Ref. [7], the values were defined prior to experiment. The values of Q_t for the $I \rightarrow (I - 2)$ transition have been calculated from the deformation of the initial state I, thereby neglecting deformation changes between the two states. Close to band termination the difference in equilibrium deformations between the I and $(I - 2)$ states becomes considerable (see Fig. 1). This suggests that the Q_t calculations are less accurate for the near-termination transitions. However, taking an average of Q_t for the initial I and final $(I - 2)$, states would only marginally affect the calculated values in the spin range, where experimental Q_t values have been extracted; thus we have used the same definition as in Ref. [7], which is expected to provide reliable results.

The excellent agreement between the experimental lifetimes and the theoretical calculations shows that the collective quadrupole moments for these three smooth terminating bands in ^{108}Sn and ^{109}Sb decrease with increasing spin. This crucial agreement, along with that for the other experimental properties, provides firm support for the cranked Nilsson model calculations which have been used to interpret smooth band termination for different configurations in a range of nuclei in this mass region. These results conclusively document, for the first time, the smooth band-termination phenomenon as the gradual transition from collective rotation towards a noncollective terminating state, where the angular momentum is limited to the sum of the aligned spins of the individual valence particle and hole constituents of the specific configuration.

We wish to thank the staff of the 88-Inch Cyclotron, A. Lipski for making the targets, and D. Ward for stimulating discussions. This work was supported by the U.S. NSF and DOE under Contract No. DE-AC03-76SF00098, the UK EPSRC, the Swedish Natural Science Research Council, AECL, and the Canadian NSERC. A. V. A. and I. R. acknowledge financial support from the Royal Swedish Academy of Sciences.

*Permanent address: Nuclear Research Center, Latvian Academy of Sciences, LV-2169, Salaspils, Miera Str. 31, Latvia.

[1] R. Wadsworth *et al.,* Phys. Rev. C **53**, 2763 (1996).
[2] J. Bron *et al.,* Nucl. Phys. **A318**, 335 (1979).
[3] V. P. Janzen *et al.,* Phys. Rev. Lett. **72**, 1160 (1994).
[4] H. Schnare *et al.,* Phys. Rev. C **54**, 1598 (1996).
[5] D. R. LaFosse *et al.,* Phys. Rev. Lett. **69**, 1332 (1992).
[6] I. Ragnarsson *et al.,* Phys. Rev. Lett. **74**, 3935 (1995).
[7] A. V. Afanasjev and I. Ragnarsson, Nucl. Phys. **A591**, 387 (1995).
[8] G. Andersson *et al.,* Nucl. Phys. A **268**, 205 (1976).
[9] J. Simpson *et al.,* Phys. Lett. B **327**, 189 (1994), and references therein.
[10] T. Bengtsson and I. Ragnarsson, Phys. Scr. **T5**, 165 (1983).
[11] T. K. Alexander and J. S. Forster, Adv. Nucl. Phys. **10**, 197 (1978).
[12] I-Y. Lee, Nucl. Phys. **A520**, 641c (1990).
[13] J. C. Wells and N. Johnson (private communication). Modified from the original code by J. Gascon (see [14]).
[14] J. Gascon *et al.,* Nucl. Phys. **A513**, 344 (1990).
[15] L. C. Northcliffe and R. F. Schilling, Nucl. Data Tables **7**, 233 (1970).
[16] D. Ward *et al.,* Chalk River Laboratories Report No. AECL-4914, 1975.
[17] T. Bengtsson and I. Ragnarsson, Nucl. Phys. **A436**, 14 (1985).
[18] A. V. Afanasjev and I. Ragnarsson, Nucl. Phys. **A608**, 176 (1997).